LAWRENCE
LIVERMORE
NATIONAL
LABORATORY

UCRL-CONF-203614

Proton Radiography as an electromagnetic field and density perturbation diagnostic

A.J. Mackinnon, P.K. Patel, R.P. Town, M.J. Edwards, T. Phillips, S.C. Lerner, D.W. Price, D. Hicks, M.H. Key, S. Hatchett, S.C. Wilks, J. King, R. Snavely, R.R. Freeman, T. Boehlly, M. Koenig, E. Martinolli, S. Lepape, A. Benuzzi-Mounaix, P. Audebert, J.C. Gauthier, M. Borghesi, L. Romagnani, T. Toncian, G. Pretzler, O. Willi

April 16, 2004

15th Topical Conference on High Temperature Plasma Diagnostics
San Diego, CA, United States
April 19, 2004 through April 22, 2004

Proton radiography as an electromagnetic field and density perturbation diagnostic

A.J.Mackinnon, P.K.Patel, R.P.Town

M.J.Edwards, T. Phillips, S.C. Lerner, D.W.Price, D. Hicks, M.H.Key, S. Hatchett, S.C.Wilks,

Lawrence Livermore National Laboratory, Livermore CA 94550, USA

J.King, R. Snavely, R.R. Freeman

University of California , Davis, CA

T. Boehlly

Laboratory for Laser Energetics, Rochester,NY, USA

M. Koenig, E. Martinolli, S. Lepape, A. Benuzzi-Mounaix, P. Audebert

Ecole Polytechnique, France

J.C. Gauthier

[6]CEA, Bruyere, Bordeaux, France

M.Borghesi, L. Romagnani

[2]Dept of Physics Queens University, Belfast, UK

T. Toncian,G.Pretzler, O.Willi

[7]Heinrich University Dusseldorf, German

ABSTRACT:

Laser driven proton beams have been used to diagnose transient fields and density perturbations in laser produced plasmas. Grid deflectometry techniques have been applied to proton radiography to obtain precise measurements of proton beam angles caused by electromagnetic fields in laser produced plasmas. Application of proton radiography to laser driven implosions has demonstrated that density conditions in compressed media can be diagnosed with MeV protons. This data has shown that proton radiography can provide unique insight into transient

electromagnetic fields in super critical density plasmas and provide a density perturbation diagnostics in compressed matter . PACS numbers: 52.50.Jm, 52.40.Nk, 52.40.Mj, 52.70.Kz

The generation of multi-MeV proton and ion beams in high intensity interactions of ultra-short laser pulses with solid targets is a rapidly growing research area. Distinctly collimated beams with cut-off energies in excess of 50MeV have been observed at high laser intensity [1]. The remarkable collimation, small transverse emittance, high cut-off energy and emission from the un-irradiated rear of the target distinguish these beams from less directed, lower energy protons observed in earlier work at lower laser intensity [2,3]. Another very important feature of these protons is that they are emitted in a timescale similar to the laser pulse duration, which is typically in the range of a few hundred femtoseconds to a few picoseconds. These properties make laser driven proton beams a unique probing tool for diagnosing electric and magnetic fields and density homogeneity in highly transient plasmas and shocked materials. In fact these proton beams have recently been used as a probe beam to investigate electromagnetic fields in plasmas [4]. In these pioneering experiments the proton beam was used as a point projection source to backlight the fields produced by the interaction of a separate laser with a solid target. Deflections in the proton backlighter were obtained from observations of localized increase in proton signal in particular areas on the spatially resolving particle detector [5]. This paper reports on the development of the new diagnostic techniques using proton beams to diagnose electromagnetic fields and density perturbations in dense plasmas.

I. Grid deflectometry using protons

Moire deflectometry is a widely used optic technique in to diagnose refractive index gradients [6] and strain in optical components[7]. Moiré effects have also been used in electron microscopy to diagnose dislocations in metals [8], and the effect has recently been demonstrated with laser driven proton beams on the JanUSP laser at Lawrence Livermore National Laboratory [11]. In optics single grid refractometry methods have also been used in conjunction with x-ray lasers to measure density gradients in laser produced plasma [12]. We will describe experiments which have utilized the development of single grid deflectometry as a technique to quantitatively measure proton

deflections from electromagnetic fields driven in laser produced plasmas[13]. This experiment was carried out on the femtosecond LULI laser at Ecole Polytechnique, France, Fig.1(a) shows a schematic of the experimental arrangement. In this experiment a 300ps duration interaction beam with 1mm wavelength and 50J energy was focused at an irradiance of 5x1015Wcm-2 onto the surface of a 125 μm tungsten wire target. The fields produced during this interaction were diagnosed by passing an MeV proton through the plasma region at 90° to the interaction beam onto a multi-layer film pack (side-on imaging). The proton beam was produced by focusing a 20J pulse, of duration 300fs and 1.054μm wavelength at a solid tungsten target at an irradiance of $1x10^{19}Wcm^{-2}$. Protons, which were accelerated from contaminants on the rear surface of the target passed through a grid before passing through the interaction plasma. By tracking the deviations of these grid elements small angular proton beam deflections can be quantitatively evaluated. Comparison of these deflections with simple proton ray tracing models allows the field structure to be extracted from the deflectograms.

Fig 1(b) shows a proton deflectogram obtained from 10MeV protons passing through the plasma,150ps before the peak of the interaction pulse. The laser is incident from the right and the plasma is the semi-spherical object roughly 200μm in diameter in the center of the image. Electromagnetic fields inside the plasma have deflection the protons in a radially symmetric manner, away from the center of the plasma. These deflections lead to apparent enlargement of the periodicity of the mesh, by roughly a factor of two. In essence the plasma is acting like a negative lens by providing a magnified image of the mesh. Another striking feature of this image is the large pile up in proton signal just on the outer boundary of the plasma. These features are both consistent with a radial electric field deflecting protons away from the center of the plasma, as will be shown in the next section.

II LSP and Lasnex simulations

The experimental images were interpreted with the aid of 2D Lasnex hydrocode [14] and LSP hybrid fluid-PIC code simulations [15]. Lasnex was used to model the evolution of the

plasma density and temperature conditions with a self consistent B fields while LSP was used to trace the proton beam through the plasma to post process the electric and magnetic field profiles to compare directly with the experimental images. As a test of the utility of proton ray tracing field as an interpretation tool for deflectometry a test problem using an analytic electric field geometry was used. Figure 2(a) shows a schematic of an LSP simulation of a point source of 7MeV protons propagating through a spherically symmetric region containing a radial E field with constant magnitude of $1x10^{9}$ Vm^{-1} and with the same transverse dimension as in the experiment. After traversing through this simulated plasma region, the protons were transported to a film pack 5cm away – as in the experiment. A simulated image at the film pack, shown in figure 2(b), closely reproduces the data with both the pile-up effect of protons at the edge of the plasma and the same apparent increase in the mesh element size inside the plasma (another feature common to both the data and the simulations is the barrel distortion of the mesh inside the plasma).

Electric field contours from a Lasnex simulation of a plasma generated by focusing a laser pulse with the experimental parameters onto a thick slab target is shown in figure 3(a). In this simulation the electric field is driven by gradients in the plasma pressure as the plasma expands radially. For the conditions of the experiment, radial fields in the range of $5\text{-}10x10^{8}$ Vm^{-1} are generated by these plasmas. LSP simulations of proton deflectometry through this field distribution produces deflections that are in good qualitative agreement with the experimental data in particular the enhanced proton signal at the plasma edge and increase in effective magnification of the mesh inside the plasma. In terms of absolute terms the deflection observed from the simulations is around a factor of two less than that in the experiment, this in turn corresponds approximately to a factor of two reduction in the observed electric field. This discrepancy may be due to the absence of suprathermal electrons in the simulation, which would be expected to generate large electric fields compared to purely thermal plasma expansion. These simulations also showed that due to the symmetry of the torroidal B field there is no contribution

to the observed deflections this geometry (in effect the deflections cancel over the line of sight of the proton probe). These issues will be discussed in more detail in a forthcoming publication.

III Proton radiography of density perturbations

Due to their large range MeV protons are also particularly suitable for radiographic applications of dense plasmas and solid materials. In particular and Multi-MeV proton beams with low emittance and short pulse length can be used to dynamically probe shocked and compressed material with high temporal and spatial resolution. For example 30-50MeV protons produced by a PW laser would be sufficiently energetic to probe cold, compressed NIF cores. Multiple scattering imposes strongly influences the imaging properties of these proton beams and in some cases limits the achievable resolution. An experiment to investigate proton probing of a laser driven implosion was carried out on the 100TW Vulcan laser system to investigate the suitability of proton radiography to diagnose overdense plasmas. As shown in figure 4(a), six beams of Vulcan (each 1μm wavelength, 1ns duration) were focused onto a microballoon at an irradiance of $1x10^{13}$ Wcm^{-2} and without phase plates. The individual beam energy was in the range of 100-150J giving a maximum energy on target of 900J. The targets were plastic microballoons (CD_2), 500μm in diameter and with two different wall thickness: 3μm and 7μm. The heater beams were arranged such that they illuminated the target tangentially from 6 orthogonal directions, giving the best symmetry this implosion.

The implosion was diagnosed by laser produced protons in the MeV range obtained by focusing a 50-100J CPA laser pulse, duration 1ps onto a solid tungsten foil at an irradiance of $5x10^{19}Wcm^{-2}$. Synchronization of the 1ns heater beams to the picosecond backlighter beam was measured to within 100ps using an optical streak camera. MeV protons were obtained from a 25μm Tungsten foil and the proton beam was characterized by an exponential spectrum of mean temperature 3MeV and a high-energy cut-off around 15-20MeV. The detector consisted of a multilayer pack containing spatially resolving dosimetry film (RCF) and particle track detectors (CR-39) as described previously. This arrangement gave a diagnostic in which each layer was

filtered by the preceding layer, giving a series of images on each shot each with a slightly different energy, ranging from 3 to 15MeV. Experimentally it was found that little or no protons were produced on shots when the back surface of the proton target was exposed to the coronal plasma surrounding the imploding balloon. To overcome this a 6mm aluminum foil was used to shield the proton foil from the hot coronal plasma produced during the implosion. This observation is consistent with the formation of a preformed plasma on the rear of the proton target before the arrival of the CPA laser pulse. Such a plasma at the rear surface of the target can reduce the accelerating electric field and disrupts the proton acceleration mechanism[5]. The aluminum pre-foil protected the back surface of the proton backlighter foil from scattered or specularly reflected light from the heater beams and low energy x-rays or fast ions from the implosion plasma and thus prevented the formation of a pre-plasma which would degrade the proton beam. A proton radiograph in 7MeV protons, of a cold (undriven) microballoon is shown in Figure 4(b). The balloon has good contrast and the shell is well resolved. Analysis of the sharpness of the edges of the balloon gives resolution ~7-10μm for this proton energy. The main limitation on the resolution in this experiment is actually due to scattering in the target rather than intrinsic emittance of the proton source. As shown in figure 5(a) the balloon impresses a 50% modulation onto the proton beam with a characteristic shape where the proton signal first reduces below the background then overshoots just outside the shell. This behavior is consistent with multiple small angle scattering of the protons as they go through the microballon wall. Also shown in fig 5(a) proton Monte-Carlo simulations of a point source propagating through the microballon using 7MeV protons. It can be seen that these simulations agree well with the data, reproducing the shape of the edge of the balloon and confirming that multiple scattering is responsible for modulating the proton beam and forming the image of the balloon.

The evolution of the capsule density profile during the implosion was studied by varying the delay between the backlighter and the implosion beams. Figure.4(c) shows a proton image of a capsule where the drive was very asymmetrical due to significant timing difference between some of the drive beams. In this case the laser beams on the left hand side of the image arrived

between 1 and 2ns before the laser beams on the right-hand-side. This led to the significant distortions with the shell traveling much further inwards on the left compared to the right. With more symmetrical drive conditions the capsule remains roughly spherical as the implosion proceeds.

Proton radiographs of shell as the implosion proceeded towards stagnation (at T_o + 3ns for this 3μm wall thickness shell), are shown in the radiograph in figure.5(c). Even though free from the gross asymmetries observed in the implosion of figure 4(c), it is clear that the implosion still suffers from significant asymmetric drive conditions. At this time the shell has assembled to peak density with a full width half maximum (FWHM) of 120μm. The stagnated shell has formed in the lower third of the original shell, consistent with higher drive energy from the upper beams, and is not spherical. Proton radiography clearly resolves the core asymmetry and allows the shape of density profile to be inferred. In order to obtain an estimate of the density profile in the core, Monte-Carlo simulations of a Gaussian shaped density featured were carried out. Figure.6(a) shows a line-out across the minor diameter of the core feature, together with the output from a Monte-Carlo simulation. The peak density of the core and the radius (fwhm) of the function were treated as variable parameters until the best match with the data was obtained. A profile with a peak density of 3g/cc and fwhm diameter of 62μm gave good agreement with the data, as shown in figure.6(a). It is clear that at this proton energy there is considerable blurring of the core, this is due to scattering of these relatively low energy protons as they traverse the core. From the simulations the blurring was negligible for higher energy protons (>12MeV) and shows that the technique is produces high resolution images of density profiles if protons of high enough energy can be produced.

The feasibility of proton radiography for diagnosing density uniformity in very dense objects such as a compressed inertial confinement fusion shell was tested by applying our Monte-Carlo model to a 1D Hydra simulation of a NIF implosion. The most important area where proton radiography could provide new or complimentary information to a fusion diagnostic such as neutron imaging is for an implosion that does not quite ignite. This implosion

may not produce enough neutrons to provide a high fidelity image of the shape of the core region and so other diagnostics must be developed which can characterize the spatial non-uniformity that prevented ignition from occurring. The density conditions in a non igniting core can still be extreme, with peak densities in the near stagnation of around 350g/cc and so one obvious candidate for this diagnostic is high energy x-ray radiography in the 20-40keV energy range. However developing x-ray techniques with the required flux and micron scale resolution are not trivial and are an ongoing research and development effort in many laboratories. Protons with energy in the 30-50MeV range could probe cores with these densities. Fig 6(b) shows a hydra profile of a "failed" indirect drive NIF implosion, where some of the shocks used to assemble the high density fuel have been mistimed. The resulting profile is typical of a stagnating imploded shell with a high density shell surrounding a hollow core. In this particular case the shell density peaks at 350g/cc at a radius of 50μm surrounding a core region with density around 50g/cc. A point projection proton image of the object in 35MeV protons is shown in fig 6(b). The full width half maximum of the dip in the proton dose is closely correlated with the location of the peak density thus showing the promise of this technique. In a real implosion other factors such as pressure gradient electric fields may also contribute to the proton dose observed on the detector although this would lead to a general deflection rather than scattering shown here. In fact the deflectometry techniques described in section I and II could be used to diagnose these fields thus providing additional information on pressure gradients in the core of an ICF target.

IV Proton radiography of shock fronts

One very important application of proton radiography is the measurement of shock fronts inside opaque materials or at the plasma vacuum interface created when a shock wave breaks out from a solid surface. Point projection proton radiography was used to investigate the density profile generated at the rear surface of a laser heated foil. The laser driving the shock in this case was part of the LULI laser; 70J pulse, 500ps in duration and focused to a spot size of 400mm giving an irradiance around $5x10^{13}Wcm^{-2}$. The protons were produce by the LULI short pulse duration

beam as described in section I and shown schematically in figure 7(a). A 10MeV proton radiograph of a shock breaking out of the rear of an aluminum target is shown in figure 7(b). This radiograph, taken 7ns after the onset of the drive pulse at the front of the target, exhibits a striking increase in proton signal at the front of the plasma produced by the shock breakout. Shock propagation through the target was diagnosed with Visar interferometry and modeled using 1D hydrodynamic codes. Monte Carlo simulations of proton propagation through hydrocode simulations of density profiles in the shock break out region cannot reproduce the proton signal enhancement at the vacuum plasma boundary. An electric field at the leading edge of the plasma is one possible source for this feature but it is unlikely that a field large enough to deflect 10MeV protons could be driven by this low (few eV) temperature plasma and so the most probable mechanism for this observation is a density profile modification caused by a phase change in the expanding plasma [16]. More detailed 2D simulations and experiments are underway to investigate these observations. Proton radiography of shock heated material is providing fundamental information on the density profile of a plasma expanding into vacuum which may be able to test theoretical models in this area.

This work was funded under the auspices of the U.S. Department of Energy by the UC/Lawrence Livermore National Laboratory under contract No. W-7405-ENF-48.

References

[1] S. P. Hatchett *et al.,* Phys. Plasmas **7**, 2076 (2000);R.A.Snavely *et al*., Phys. Rev. Lett **85**, 2945 (2000);E.L. Clark *et al.,* Phys. Rev. Lett **84**, 670 (2000);A. Maksimchuk *et al*., Phys. Rev. Lett. **84**, 4108 (2000); K. Nemoto et al., Appl. Phys. Lett. **78**, 595-597 (2001);Y. Murakami, *et al*., Phys. Plasmas (2001).

[2] S.J.Gitomer, Phys. Fluids **29**, 2679 (1986). A.P. Fews, *et al*., Phys. Rev. Lett **73**, 1801 (1994), F.N. Beg *et al.,* Phys. Plasmas **4**, 447 (1997).

[3] J.E.Crow, P.L. Auer and J.E.Allen, J. Plasma Physics **14**, 65 (1975). J. Denavit, Phys. Fluids **22**, 1385 (1979). Y. Kichimoto, *et al*., Phys. Fluids **26**, 2308 (1983).

[4] M. Borghesi et al., Plasma Phys. Cont. Fusion, (2001)

[5] M. Borghesi et al., Phys. Plasma (2002)

[6] O.Kafri, Opt.Lett, 5,555 (1980),O.Kafri and I Glatt, Opt. Eng. 24, 944 (1985)

[7] O.Kafri and I. Glatt, *The Physics of Moiré Metrology* , Wiley (1990) and references therein.

[8] P.Theocaris, Moiré Fringes in strain analysis Permagon Press, Oxford (1969)

[9] D.W.Pashley,J.W. Menter, G.A.Basset, Nature, **179**, 752 (1957)

[11] A.J.Mackinnon et al., App. Phys. Lett. 82, (2003), A.J.Mackinnon et al., Rev Sci Instrumen 74 1917 part 2 Sp. Iss. (2003)

[12] Takahashi K, Kodama R, Tanaka KA, et al., Phys. Rev. Lett 84 2405 (2000).

[13] G. Pretzler et al.,Submitted to Science

[14] G. B. Zimmerman, W. B. Kruer, Comm. Plasm. Physics and Controlled Fusion, 2 (1975) 51.

[15] D.R. Welch, et al, Nucl. Inst. Meth. Phys. Res. A 464, 134 (2001).

[16] M. Koenig et al., submitted to Nuc Fusion (2004).

Figures:

1. (a) Schematic of Deflectometry experiment undertaken on the LULI laser at Ecole Polytechnique, France. The interaction beam creates a plasma which is then probed by protons created by a second femtosecond laser pulse focused onto a surrogate target. The proton beam is broken up into hundreds of small beamlets as it passes through a 1500lpi mesh before traversing the plasma

   (b) 7 MeV Proton image showing distortions of the mesh as the protons pass through the plasma region

2. Hybrid PIC code simulations of protons traversing a spherically symmetric region containing a radial electric field.
   (a) Geometry of the simulation, the region has the same transverse dimensions as the experimental plasma and the relative positions of the proton source and detector match the experiment.
   (b) Simulated Image on film pack. The distortions in the mesh closely match the experimental data shown in (c), in terms of; the radially symmetric increase in effective magnification of the mesh elements inside the plasma; the pile up in proton signal at the outer edges of the plasma and the barrel type distortion of the mesh elements inside the plasma.
   (c) Experimental data
3. Lasnex and LSP simulations of the experimental parameters
   (a) Radial electric fields calculated from the radial pressure gradient term obtained from Lasnex simulations of the deflectometry experiment
   (b) Proton density plot at the image plane from hybrid LSP code proton trajectories of 7MeV protons that have traversed the Lasnex calculated electric fields.
4. Proton radiography of laser driven implosions.

(a) The implosion and backlighting geometry. 6 beams of the Vulcan laser at Rutherford Appleton laboratory were used to drive an implosion of 500mm microballoons. Proton radiography was used to diagnose the temporal evolution of the implosion

(b) Proton radiograph in 7MeV protons of a cold microballoon

(c) Proton radiograph of an asymmetric implosion. Timing differences in 3 of the heater beams have caused strong density non uniformities to develop.

5 (a) Lineout of proton dose through the cold shell plus Monte Carlo simulations based on SRIM calculations.

(b) Proton radiograph of a compressed shell close to stagnation

(c) Lineout through core region

6. (a) Lineout core shown in fig 5(b) and Monte Carlo simulation of a spherically symmetric core with a Gaussian density profile; peak density3g/cc and 62μm FWHM

(b) 1D Monte-Carlo simulation of proton radiograph of a mistimed NIF shot which failed to ignite. The density profile was generated from 1D hydrocode – Hydra.

7. (a) Schematic of proton radiograph experiment to diagnose the plasma produce by shock breakout

(b) Proton Radiograph of the plasma produced 7ns after the shock began propagating through a 15μm Aluminum foil

(a)

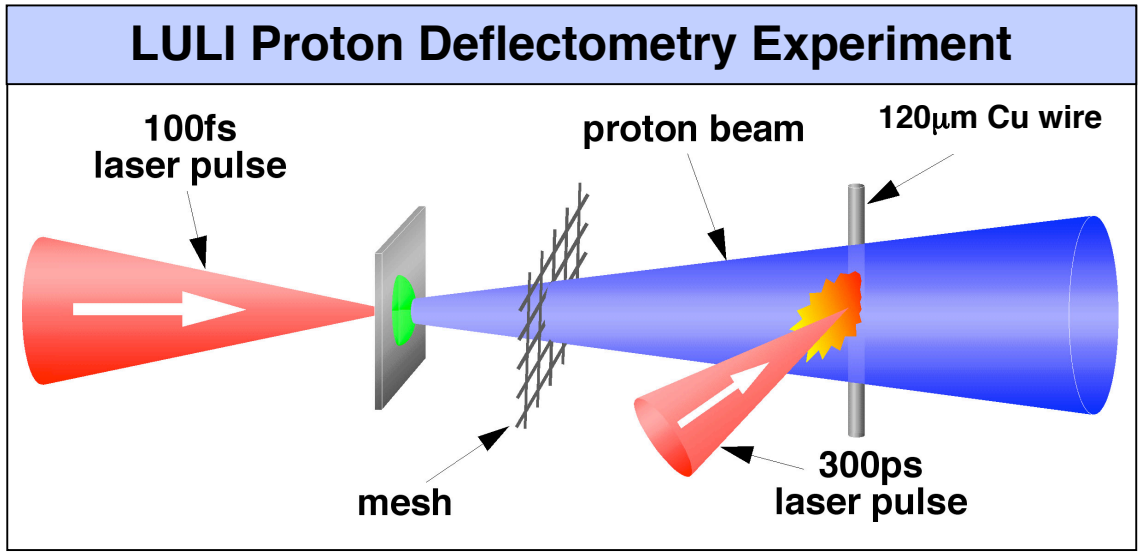
LULI Proton Deflectometry Experiment
100fs
laser pulse
proton beam
120μm Cu wire
mesh
300ps
laser pulse

(b)

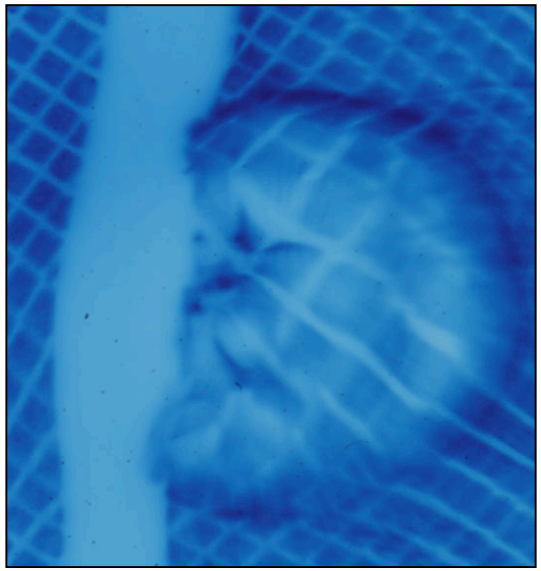

Figure 1

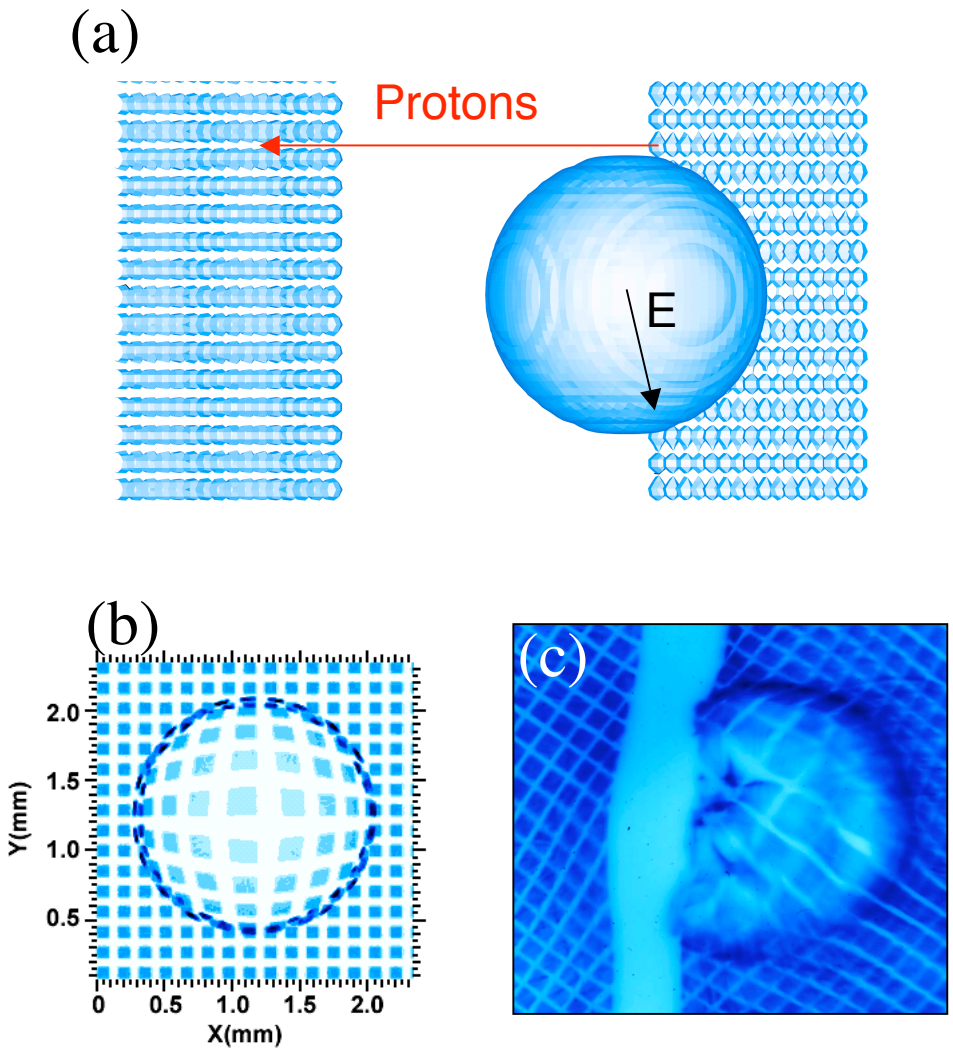

Figure 2

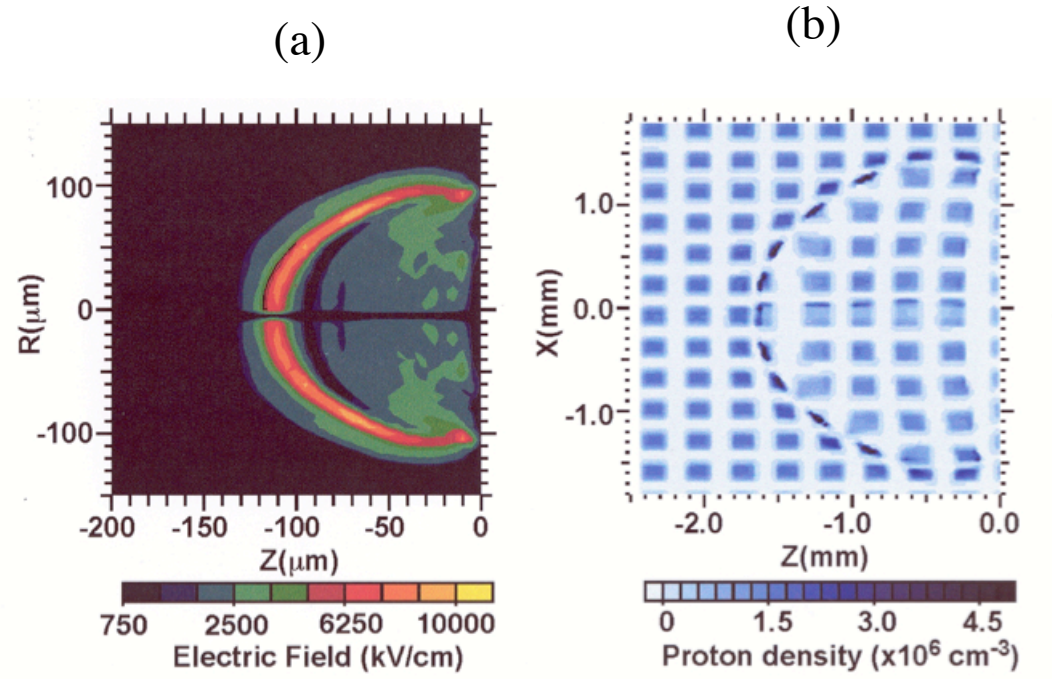
(a)
(b)
100
0
-100
R(μm)
-200
-150
-100
-50
0
Z(μm)
750
2500
6250
10000
Electric Field (kV/cm)
1.0
0.0
-1.0
X(mm)
-2.0
-1.0
0.0
Z(mm)
0
1.5
3.0
4.5
Proton density (x10^6 cm^-3)

Figure 3

(a)

Heaters: λ = 1μm, 6x50J @ 1ns, 1μm
Target: 500μm diameter balloon;3 or 7μm wall thickness

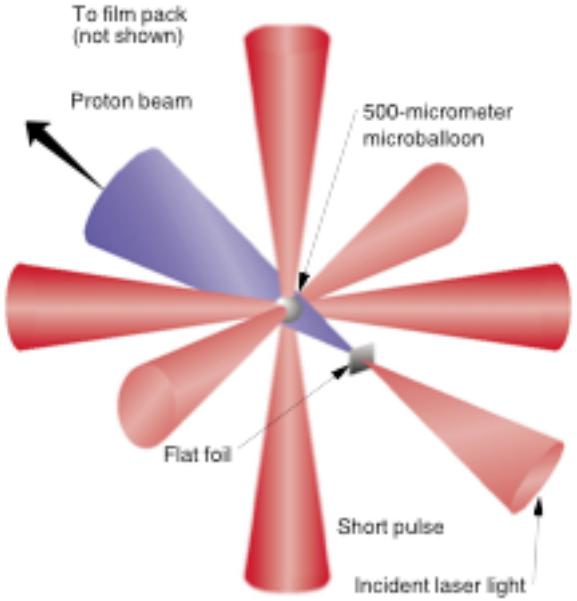

Static target

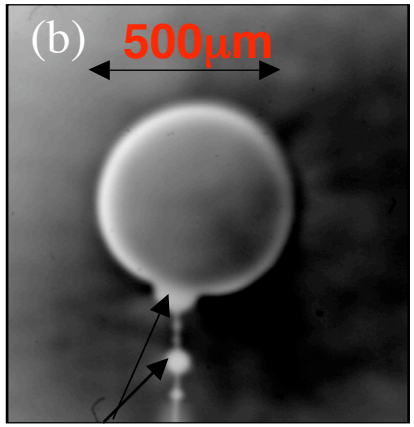

Glue

Asymmetric drive

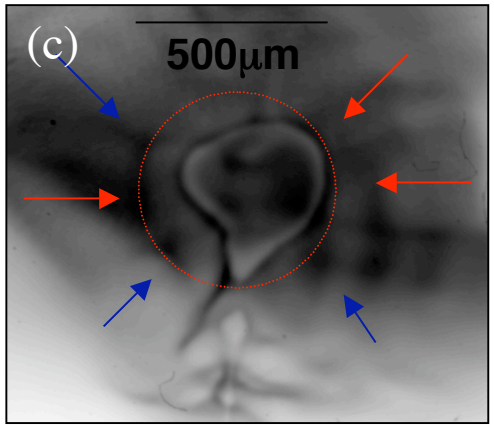

To + 1-5ns*
(*heaters early)

Figure 4

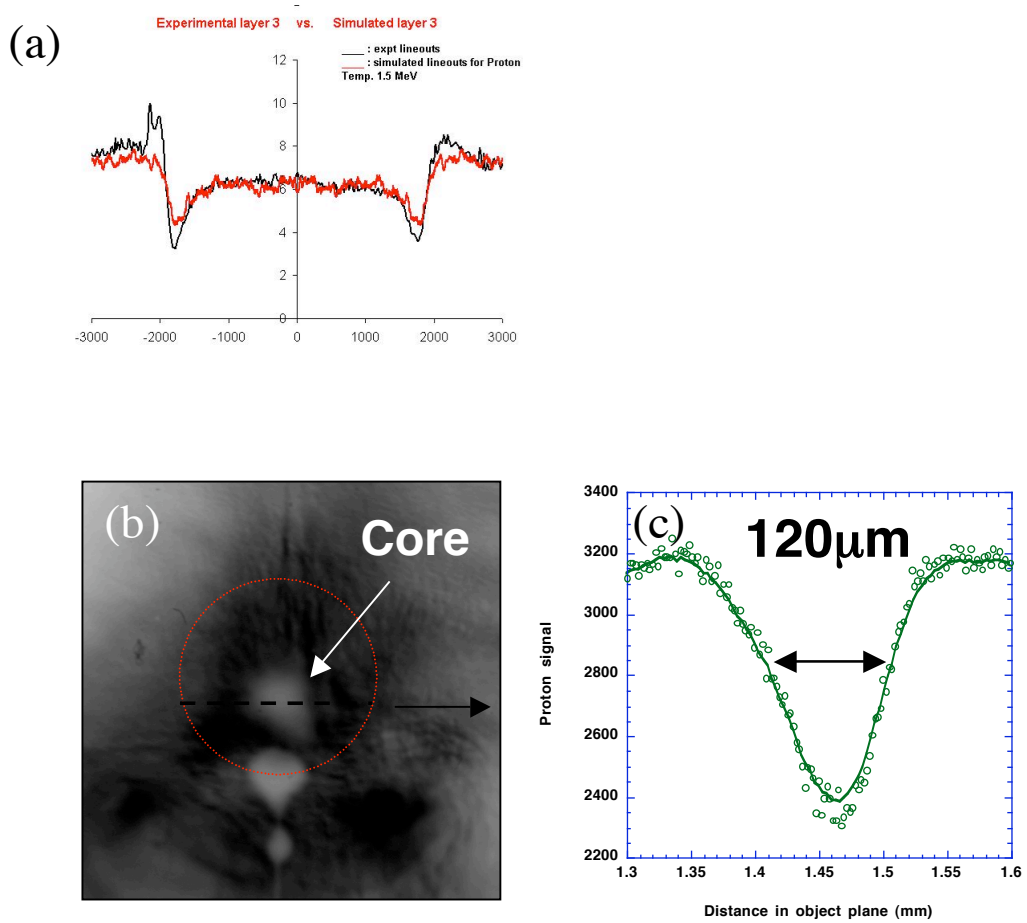
(a)
Experimental layer 3 vs. Simulated layer 3
: expt lineouts
: simulated lineouts for Proton
Temp. 1.5 MeV
12
10
8
6
4
2
0
-3000
-2000
-1000
0
1000
2000
3000
(b)
Core
(c)
120μm
Proton signal
3400
3200
3000
2800
2600
2400
2200
1.3
1.35
1.4
1.45
1.5
1.55
1.6
Distance in object plane (mm)

Figure 5

(a)

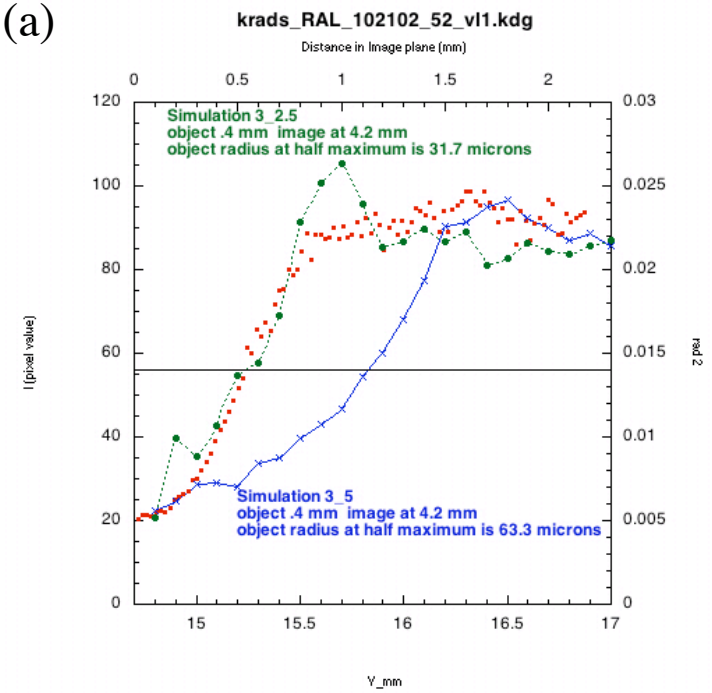
krads_RAL_102102_52_vl1.kdg
Distance in Image plane (mm)
Simulation 3_2.5
object .4 mm image at 4.2 mm
object radius at half maximum is 31.7 microns
Simulation 3_5
object .4 mm image at 4.2 mm
object radius at half maximum is 63.3 microns
I (pixel value)
rad 2
Y_mm

(b)

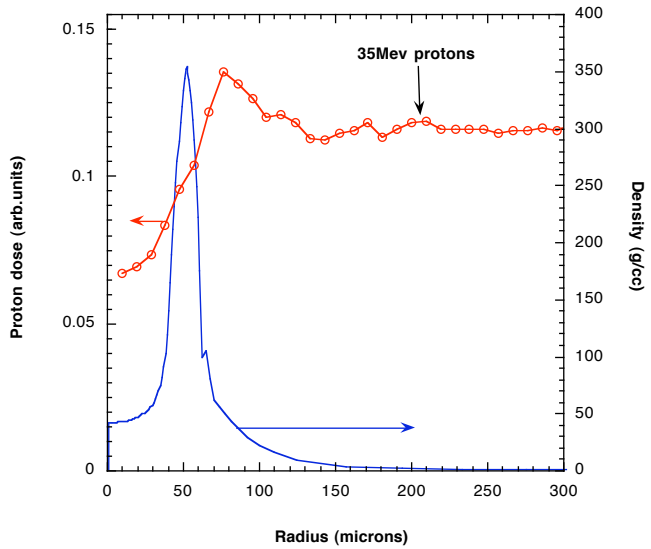
35Mev protons
Proton dose (arb.units)
Density (g/cc)
Radius (microns)

Figure 6

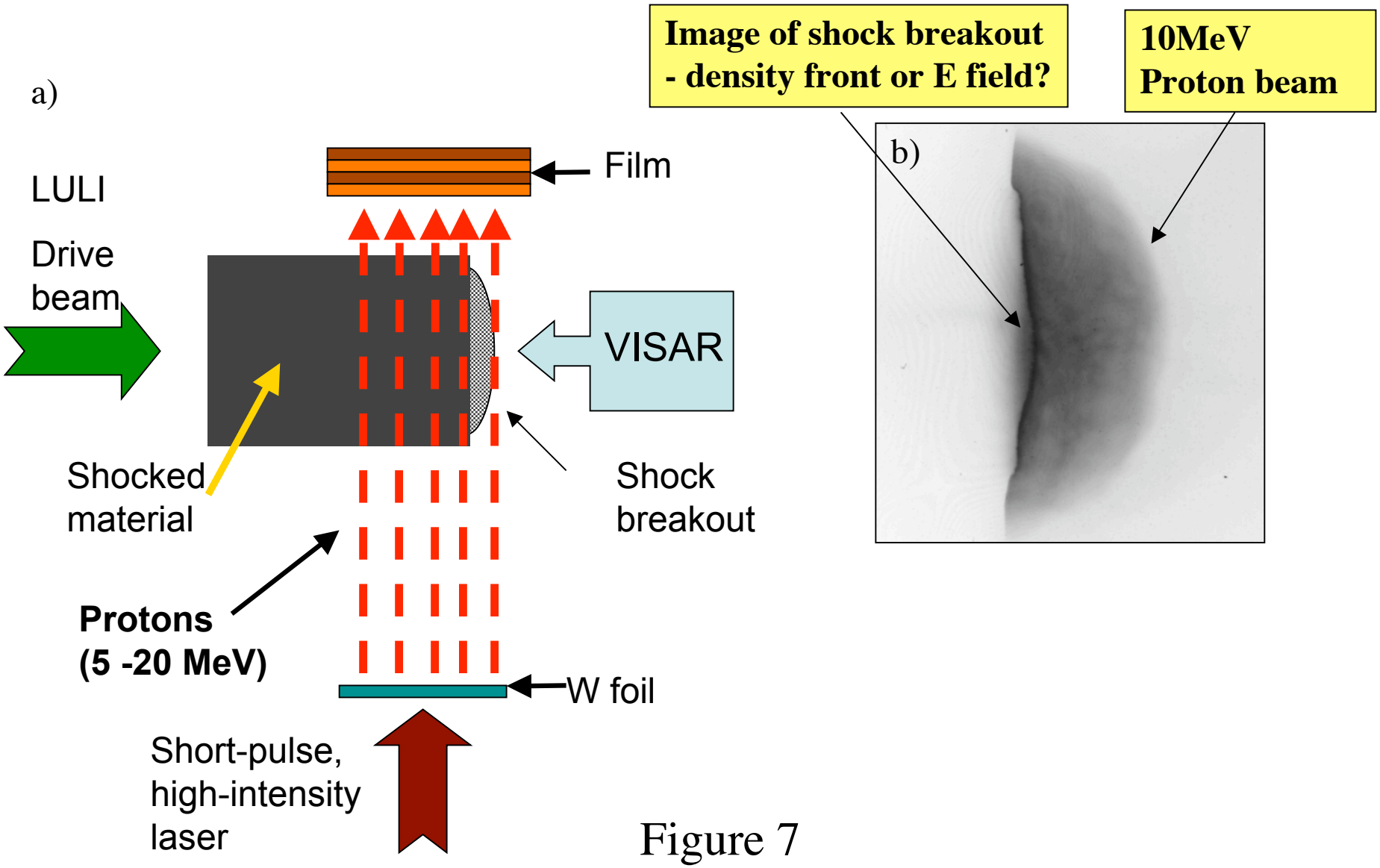
a)
LULI
Drive beam
Film
VISAR
Shocked material
Shock breakout
Protons
(5 -20 MeV)
W foil
Short-pulse, high-intensity laser
Image of shock breakout - density front or E field?
10MeV Proton beam
b)

Figure 7